

Functional Pyrene–Pyridine-Integrated Hole-Transporting Materials for Solution-Processed OLEDs with Reduced Efficiency Roll-Off

Krishan Kumar,¹ Kiran Kishore Kesavan,¹ Diksha Thakur, Subrata Banik, Jayachandran Jayakumar, Chien-Hong Cheng, Jwo-Huei Jou,* and Subrata Ghosh*



Cite This: *ACS Omega* 2021, 6, 10515–10526



Read Online

ACCESS |



Metrics & More

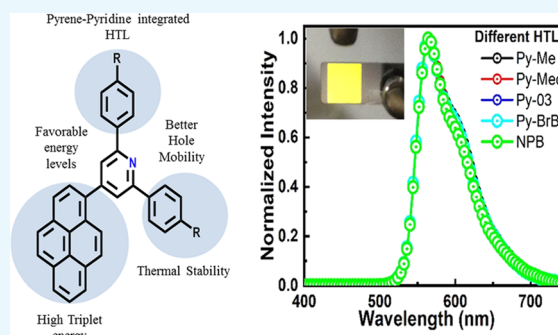


Article Recommendations



Supporting Information

ABSTRACT: A series of new functional pyridine-appended pyrene derivatives, viz., 2,6-diphenyl-4-(pyren-1-yl)pyridine (**Py-03**), 2,6-bis(4-methoxyphenyl)-4-(pyren-1-yl)pyridine (**Py-MeO**), 4-(pyren-1-yl)-2,6-di-*p*-tolylpyridine (**Py-Me**), and 2,6-bis(4-bromophenyl)-4-(pyren-1-yl)pyridine (**Py-Br**) were designed, developed, and studied as the hole-transporting materials (HTMs) for organic light-emitting diode (OLED) application. The crystal structures of two molecules revealed to have a large dihedral angle between the pyrene and pyridine units, indicating poor π -electronic communication between them due to ineffective orbital overlap across the pyrene–pyridine systems as the two p-orbitals of pivotal atoms are twisted at 66.80° and 68.75° angles to each other in **Py-03** and **Py-Me**, respectively. The influence of variedly functionalized pyridine units on the electro-optical properties and device performance of the present integrated system for OLED application was investigated. All of the materials have suitable HOMO values (5.6 eV) for hole injection by closely matching the HOMOs of indium tin oxide (ITO) and the light-emitting layer. All of the synthesized molecules have suitable triplet energies, glass transition temperatures, and melting temperatures, which are highly desirable for good HTMs. The pyrene–pyridine-based devices demonstrated stable performance with low-efficiency roll-off. The device with **Py-Br** as HTM showed a maximum luminance of 17300 cd/m² with a maximum current efficiency of 22.4 cd/A and an EQE of 9% at 3500 cd/m² with 7% roll-off from 1000 to 10 000 cd/m². Also, the devices with **Py-Me** and **Py-03** showed performance roll-up while moving from 1000 to 10 000 cd/m².



INTRODUCTION

Since the first demonstration of light emission by Tang and Van Slyke in 1987,^{1,2} the organic light-emitting diodes (OLEDs) have attracted much attention in terms of both material synthesis and device fabrication. In recent years, great progress has been made toward highly efficient and long-lifetime OLEDs.^{3–6} Due to superior performance, high brightness, quick response, high-speed video rate, and flexibility of OLEDs,^{7–14} their development has received wide attention of researchers from academia to industry.^{15,16} For the constant demand for highly efficient organic light-emitting devices, the application of new materials in electroluminescence display has become a very interesting topic in chemistry and applied physics. High-performance OLED devices can be obtained by building the multilayer structure¹⁷ comprising of an ITO glass substrate anode, a hole-transporting material (HTM), an electron-transporting material (ETM), and a cathode.¹ One approach that has been widely used to achieve an efficient OLED device is the effective hole-transporting layer, which decreases the energy barrier between the anode and an organic emitter in a multilayer structure.^{17–20} Therefore, there has been a strong focus on developing new hole-transporting materials to achieve good

OLED devices. Generally, an excellent hole-transporting material for electroluminescence diode application should demonstrate good hole mobility for positive charge carriers to migrate from the anode to the emissive layer, a proper HOMO energy level to ensure a low energy barrier for the hole injection from the hole-transporting layer to the emissive layer, morphologically stable thin film, and high thermal stability.^{21–23}

During the past few years, several carbazole, triphenylamine, phenoxazine, and tolylamino cyclohexane-based compounds have been studied as hole-transporting materials in electronic devices because of their good electron-donating properties and suitable hole mobility.^{24–33} In early stage, the aryl-amine derivatives such as *N,N'*-diphenyl-*N,N'*-bis(1-naphthyl)-(1,1'-biphenyl)-4,4'-diamine (NPB), 1,1-bis((di-4-tolylamino)-cyclohexane (TAPC), and *N,N'*-bis(3-methylphenyl)-*N,N'*-bis-

Received: August 24, 2020

Accepted: December 15, 2020

Published: April 15, 2021



(biphenyl)benzidine (TPD) were the most widely used HTMs.^{34–36} The triphenylamine- and carbazole-based derivatives such as 4,4',4''-tris((3-methylphenyl)phenyl-amino)-triphenylamine (*m*-MTDATA),³⁷ (9,9'-bis(4-vinylbenzyl)-9*H*,9*H*'-3,3'-carbazol) (VvPyMCz),³⁸ and 1,3-bis(*N*-carbazolyl)benzene (mCP)³⁹ are also used as good HTMs. Small molecule-based HTMs are relatively easy to synthesize, which in turn reduces the fabrication cost of OLED devices. The materials based on triphenylamine and carbazole have estimable properties including large triplet state energy, high chemical and thermal stability, which make them promising materials for OLED devices. However, the crystallization of some of the aryl-amine-based materials during film-formation in the solution process as well as their performance at high temperature have become restricting factors for their OLED applications.³² On the other hand, the isolated carbazole and triphenylamine ring containing materials have high ionization potentials that are not appropriate for the hole-transporting layer.^{32,40}

Among the many reported materials, pyrene has strong electron delocalization and fused conjugated aromatic ring systems in its architecture.⁴¹ Therefore, pyrene acts as a good light emitter as well as a hole transporter. Pyrene is a source for organic optoelectronic materials and has been used as a hole transporter in OLEDs and perovskite solar cells.⁴¹ Cui et al. reported pyrene-based HTMs for perovskite solar cells with the best PCE of 19.20%.⁴² To date, many kinds of functionalized pyrene-based materials have been synthesized, and some of them proved to be good hole transporter for OLEDs.^{43–47} Recently, Chang et al. reported pyrene derivatives 2-(4-(pyren-1-yl)phenyl)-9-hexylcarbazole and *N*1,*N*6-di([1,1'-biphenyl]-4-yl)-*N*,*N*6-bis(9,9-dimethyl-9*H*-fluoren-2-yl)pyrene-1,6-diamine (PyFB) and used them as hole-transporting materials in red phosphorescent and blue fluorescent organic light-emitting diodes, respectively.^{43,44} It was found that PyFB showed better hole-transporting properties than a commercially available (NPB) material. Keawin et al. have synthesized pyrene-based multifunctional materials that behave as blue emitters and hole-transporting materials in OLEDs.⁴⁶ On the other hand, Salunke et al. synthesized a pyrene derivative 4,4',4'',4'''-(pyrene-1,3,6,8-tetra-yl)tetrakis(2-fluoro-*N,N*-bis(4-methoxyphenyl)aniline) (L-F) and used it as a hole-transporting material with excellent green emission.⁴⁵ Although, NPB and *N,N'*-diphenyl-*N,N'*-bis-(1-naphthyl)-1,10-biphenyl-4,4-diamine (NPD) are commercially available widely used HTMs for OLED fabrication, Loy et al. have reported that NPD faces irreversible failure when heated due to crystallization.⁴⁸ Moreover, in recent time, rationally functionalized pyridines have been investigated to have good hole extraction and hole-transporting potential, and thus, such materials have been used as efficient hole-transporting materials (HTMs) for optoelectronic applications.^{49–54} While different types of pyrene and pyridine derivatives have been developed and tested for their potential as HTMs, there has been no report, to our knowledge, on the use of pyridine–pyrene-integrated systems as HTMs for optoelectronics applications.

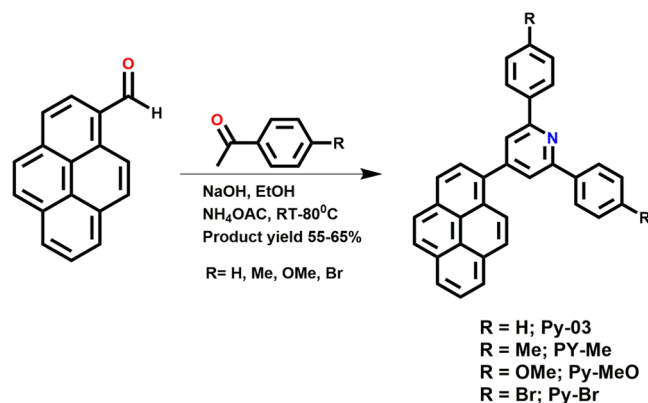
In this study, we are demonstrating a novel electroactive material series containing poor orbital overlap-driven electronically isolated pyrene ring. The pyrene-functionalized hole-transporting materials are less explored in OLEDs. The present pyridine-substituted pyrenes have been prepared by a condensation reaction, and they have shown good device

performance at low driving voltage. In these new pyridine-appended pyrene derivatives, pyrene acts as a donor and pyridine acts as an acceptor. The diphenyl unit of pyridine is substituted with different functional groups such as –OMe, –Me, and –Br. It has been reported that the presence of such functional groups in the molecular structure improves device performance by tuning molecular properties.^{55–57} As reported in the literature, the introduction of halogen atoms into the chemical structure changes the carrier mobility of the molecules.^{58–61} While using these compounds as HTL in yellow OLED, the Py-Br showed good EQE (9%) and a maximum luminance of 17 300 cd/m² with low-efficiency roll-off. Interestingly, all four molecules exerted high operating stability and low roll-off. Further, they exhibited very good thermal stability and suitable HOMO/LUMO energy levels, making them promising hole transporters. As these materials have a well-matched HOMO/LUMO level (5.6/2.3 eV) for hole injection with lower ionization potentials, they could be used as hole-transporting and injection materials in OLED devices.

RESULTS AND DISCUSSION

A simple condensation method was adopted to synthesize 1-substituted pyrenes. The condensation between pyrene-1-carboxaldehyde and aryl ketones in the presence of ammonium acetate resulted in the formation of desired substituted pyrenes (Scheme 1). Initially, pyrene-1-carboxaldehyde undergoes

Scheme 1. Synthetic Route for PY-03, Py-MeO, Py-Me, and Py-Br



condensation with four different kinds of acetophenone derivatives in the presence of sodium hydroxide to yield α,β -unsaturated compounds as an intermediate, which further undergoes cyclization in the presence of ammonium acetate to produce desired pyrene derivatives **Py-03**, **Py-MeO**, **Py-Me**, and **Py-Br**.⁶² All of the synthesized molecules were purified by column chromatography and characterized by mass spectrometry, ¹H, and ¹³C NMR, and the spectroscopy data were in agreement with expected molecular structures. Besides, the structural integrity of two compounds, viz., **Py-03** and **Py-Me** was established through single-crystal structure analysis. The end compounds showed good solubility in common organic solvents.

Optical Properties. The optical properties of **Py-03**, **Py-MeO**, **Py-Me**, and **Py-Br** were examined by measuring absorption and emission spectra in dichloromethane (DCM) at room temperature. The ultraviolet–visible (UV–vis) spectra

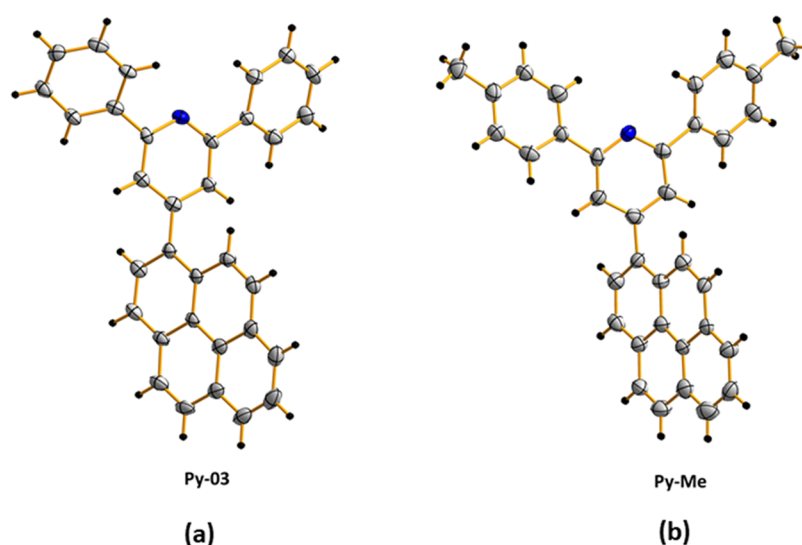


Figure 1. ORTEP diagrams of (a) Py-03 and (b) Py-Me.

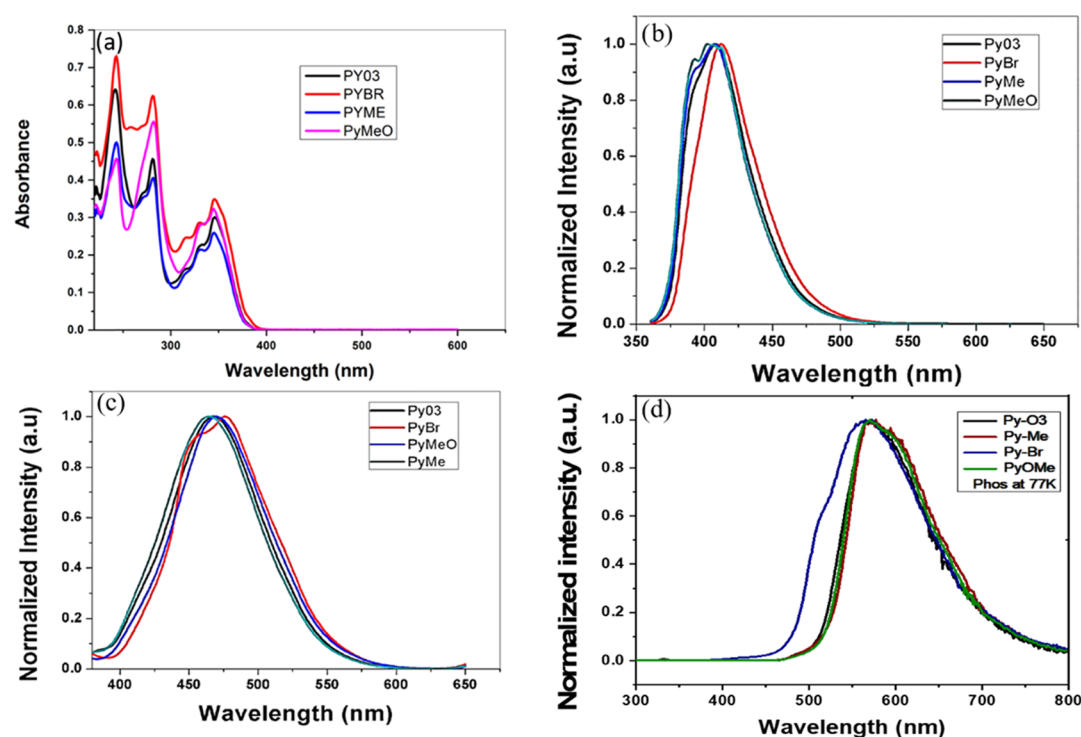


Figure 2. (a) UV-vis and (b) photoluminescence (PL) spectra of Py-03, Py-MeO, Py-Me, and Py-Br in DCM; (c) PL spectra of the thin films of Py-03, Py-MeO, Py-Me, and Py-Br; and (d) PL spectra of Py-03, Py-MeO, Py-Me, and Py-Br measured at low temperatures (77 K).

Table 1. Optical, Electrochemical, and Thermal Properties of All Compounds

s. no.	λ_{abs}^a (nm)	λ_{em}^b (nm)	HOMO ^c (eV)	LUMO ^c (eV)	E_g^d (eV)	E_T^e (eV)	T_m^f (°C)	T_5d^g (°C)
Py-03	242/280/345	469/408	-5.63	-2.35	3.28	2.49	190	357
Py-MeO	242/280/344	469/404	-5.61	-2.33	3.28	2.46	200	355
Py-Me	242/280/344	464/408	-5.63	-2.33	3.30	2.45	210	367
Py-Br	242/280/344	478/412	-5.65	-2.39	3.26	2.62	245	249

^aMeasured in dichloromethane (DCM) at room temperature. ^bMeasured in the solid state and solution phase. ^cMeasured from oxidation onset of CV and LUMO energy levels were estimated from HOMO levels and E_g . ^d E_g was determined from the absorption onset. ^e E_T (triplet energy) was calculated from the onset of the phosphorescence spectrum at 77 K. ^fDetermined from DSC (T_m is the melting temperature). ^gEstimated from a thermogravimetric analyzer (T_5d with a 5% weight loss).

of the organic compounds are displayed in Figure 2, and the related data are listed in Table 1.

The UV-vis absorption behavior of all of the pyrene-based molecules (13.5 μM) was studied to get an idea of the extent

of π - π conjugation and charge-transfer properties.⁶³ It was observed that the UV-vis absorption behavior and optical band gaps of all of these molecules were nearly the same. This indicated that the substitutional change at the pyridine ring did not have much impact on the electronic properties of these molecules, which were also supported by the DFT results. This is probably due to the poor electronic conjugation through the mesomeric effect between pyrene and pyridine units as the pivotal p-orbitals are more than 60° twisted around each other, indicating ineffective orbital overlap, which is otherwise required for π - π conjugation. Three different kinds of bands were observed in the range of 242–345 nm. The high energy band was observed with a maximum at 242 nm and the low-energy band tailed up to 395 nm with a maximum around 345 nm (Figure 2). From the DFT and crystal structure analyses, it was observed that both pyrene and pyridine are almost distinct units (i.e., the electron delocalization within the molecule is not uniform). So, the photophysical behavior of all of the pyrene-pyridine-based molecules is dependent on both the units. However, the absorption spectra profile of all of these compounds (Figure 2) resemble to a greater extent with the absorption spectra of pyrene or substituted pyrene.⁶⁴ Hence, the most prominent bands at ~242, 280, and 345 nm are due to π - π^* transition in the pyrene unit. Note that all of the absorption peaks due to π - π^* transition were evident from their high extinction coefficient (ϵ) values (>20 000).

The fluorescence spectra of all of the compounds were recorded both in solutions and solid states. The PL spectra of the synthesized compounds are displayed in Figure 2, and the relevant data are listed in Table 1. The fluorescence spectra in the solution state were measured in the DCM solution, and their corresponding emission peak maxima were 408, 404, 408, and 412 nm for Py-03, Py-MeO, Py-Me, and Py-Br, respectively. The optical band gaps (E_g) of these compounds were determined from the onset of the absorption spectra, and all of the synthesized compounds Py-03, Py-MeO, Py-Me, and Py-Br showed E_g of 3.28, 3.28, 3.30, and 3.26 eV, respectively. The thin-film PL spectra of all of the compounds were recorded after preparing the film on a quartz substrate by the drop-casting method. The thin-film PL spectra of all of the compounds were noticed to be red-shifted by 56–66 nm as compared to those in the solution. The red shift in thin-film PL spectra is possibly due to intermolecular interactions between the molecules in the solid states. In general, the intermolecular interactions are more in the solid state as compared to the solution state. Pyrene-pyridine is a nonplanar integrated system in the ground state, which may attain some extent of planarity in the excited state, resulting in greater intermolecular interaction and conjugation.^{65,66}

Electrochemical and Thermal Studies. The electrochemical properties of the synthesized compounds were examined by cyclic voltammetry (CV) using a standard three-electrode electrochemical cell with tetrabutylammonium hexafluorophosphate as the electrolyte. The reference electrode was Ag/AgCl, the working electrode was a platinum disc, and the counter electrode was a platinum wire. The highest occupied molecular orbital (HOMO) energy levels calculated using oxidation potentials obtained from cyclic voltammetry are summarized in Table 1, and the spectra are presented in Figure S1. The estimated HOMO energy levels of Py-03, Py-MeO, Py-Me, and Py-Br are -5.63, -5.61, -5.63, and -5.65 eV, respectively, and their corresponding lowest unoccupied molecular orbital (LUMO) energy levels are -2.35, -2.33,

-2.33, and -2.39 eV, which are calculated by subtracting the HOMO levels from the energy gap obtained from the absorption spectra. The HOMO values of all of the compounds are nearly the same because they share the same chemical platform of a pyrene ring. Accordingly, from the HOMO and LUMO levels, the optical energy gaps were determined to be nearly 3.28 eV. All of these values indicated that the present set of pyrene-pyridine derivatives possesses suitable energy levels to be used as hole-transporting and injection materials in OLEDs.⁴⁷

The thermal stability and the behavior under heating of the synthesized materials were investigated using TGA and DSC under a nitrogen atmosphere. The TGA and DSC graphs are represented in Figure S2, and the related data are listed in Table 1. TGA analysis revealed that the present pyrene-pyridine derivatives have high thermal stability as their decomposition temperatures corresponding to a 5% weight loss are very high (Table 1 and Figure S2). As evident from the TGA graph, the decomposition temperature corresponding to the 5% weight loss was calculated to be 357 °C for Py-03. Similarly, Py-MeO and Py-Me showed the decomposition temperatures corresponding to the 5% weight loss at 355 and 367 °C, respectively. Further, the decomposition temperature with the 5% weight loss of Py-Br was found to be 249 °C. In general, the thermal stability of a molecule depends on the strength of the bond present in the molecule.⁶⁷ The lower thermal stability of Py-Br is possibly due to the presence of weak C-Br bond as compared to C-C, C-O, and C-H bonds (present in other molecules). Meanwhile, the corresponding glass transition temperatures (T_g) were determined from DSC to be 155 and 202 °C for Py-03 and Py-Br (Figure S2e,h), respectively; however, no clear T_g was observed for Py-MeO and Py-Me. The melting temperatures (T_m) were also determined from DSC for all of the compounds to be 190, 200, 210, and 245 °C for Py-03, Py-MeO, Py-Me, and Py-Br (Figure S2), respectively. The high value of T_g and T_m implies that the synthesized materials possess good morphological stability and thus can be used as stable materials for optoelectronics devices.

Theoretical Level of Understanding. To understand the correlation between electronic structure and electrochemical and photophysical properties of the developed compounds, the density functional theory (DFT) calculations were performed using the hybrid functional B3LYP along with 6-311G(d,p) basis set. All of these calculations have been done in the solvent phase (DCM) using Gaussian03 software. The optimized structure of compound Py-Br is represented in Figure 3, and the optimized structures of Py-03, Py-MeO, and Py-Me are given in Figure S3.

The distributions of HOMOs and LUMOs are depicted in Figures 3 and S3. The calculated HOMO energy values of Py-03, Py-MeO, Py-Me, and Py-Br are -5.73, -5.71, -5.72, and -5.76 eV, respectively, and the corresponding LUMO energy values are -2.06, -2.03, -2.04, and -2.12 eV. Since the singlet and triplet energy levels of the hole-transporting materials play a crucial role in device performance, the time-dependent DFT (TD-DFT) calculations were carried out to get the theoretical values of singlet and triplet energies at the same level of the theoretical method and basis set. The theoretical UV-vis spectrum in the gas phase is represented in Figure S4. The calculated high-intensity peaks of the theoretical UV-vis spectra appear at 367, 374, 366, and 364 nm for Py-03, Py-Br, Py-Me, and Py-MeO, respectively. These

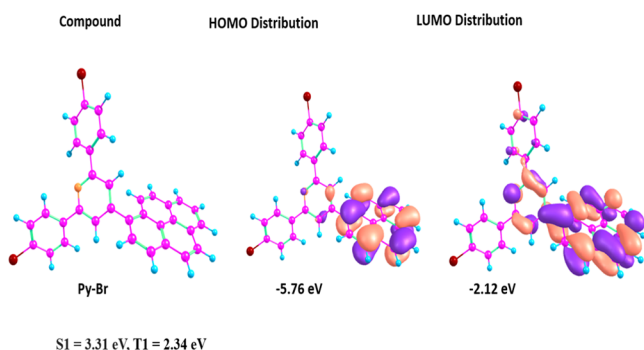


Figure 3. Optimized structure and HOMO/LUMO distribution of Py-Br.

transitions may be attributed to $\pi-\pi^*$ transitions. It was noted that the strong electron-withdrawing effect of the bromo group possibly caused a red shift in the absorption peak as compared to Py-03, while methyl and methoxy units being electron donating in nature caused a little blue shift in an absorption peak as compared to Py-03. The calculated energy values of the singlet states (S1) for Py-03, Py-MeO, Py-Me, and Py-Br are 3.38, 3.37, 3.39, and 3.31 eV, respectively, and energies of the triplet (T1) states are 2.35, 2.35, 2.35, and 2.34 eV for Py-03, Py-MeO, Py-Me, and Py-Br, respectively.

Device Performance. The good thermal and photo-physical properties of these structurally engineered pyrene-pyridine compounds inspired us to incorporate these as the hole-transporting layer (HTL) in solution-processed OLED devices. The schematic illustration of the OLED device structure is represented in Figure 4.

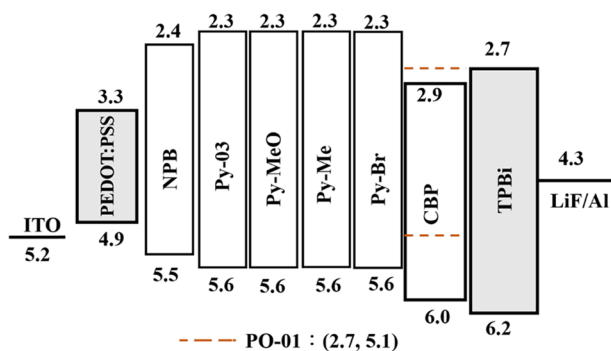


Figure 4. Schematic illustration of solution-processed OLED devices consisting of different HTLs.

The complete description of the device fabrication process has been provided in **Experimental Section**. To investigate the surface morphology of the solution-processed PEDOT:PSS, PEDOT:PSS/Py-Br, and PEDOT:PSS/Py-Br/EML thin films, their AFM images have been recorded in the tapping mode (Figure 5). It is notable that all of the deposited single- and multilayered films are uniform and pinhole-free. The respective root-mean-square (R_{RMS}) surface roughness values are 1.2, 1.0, and 0.78 nm. Interestingly, the R_{RMS} value of the emissive layer is lower than the HTL layer, indicating that it is not dissolved into the HTL layer during the successive deposition. However, managing the no-mixing of adjacent layers of solution-processed devices is a real challenge, and hence, researchers are involved in developing approaches to address this issue. Therefore, for the present case, a certain extent of mixing at the interfaces cannot be overruled.

Electroluminescent properties of all of the devices are represented in Figure 6; all of the devices represent very similar turn-on (3 V) voltage with almost indistinguishable emission spectrum (562 nm). The summarized performances of all of the devices are represented in Table 2. Among all of the devices, a Py-Br-based device exerted the highest EQE of 9% followed Py-MeO (8.8%), Py-03 (8.5%), Py-Me (8.5%), and NPB (6.7%). On the other hand, NPB-based devices showed the highest power efficiency (PE) (20.3 lm/W)—among all the devices, whereas Py-Br-based devices exhibited the highest current efficiency (27.6 cd/A) among all of the devices, as demonstrated in Table 2.

Interestingly, in the case of all of the pyrene-pyridine-based devices, the maximum performances were observed at higher luminescence (3500 cd/m²). In brief, maximum CE and PE were observed at higher luminescence at 3500 cd/m² (Py-Br: 27.6 cd/A and 12.3 lm/W; Py-MeO: 25.7 cd/A and 11.8 lm/W; Py-03: 26.6 cd/A and 11.8 lm/W; and Py-Me: 25.2 cd/A and 11.4 lm/W). In contrast, the reference device with NPB exhibited the maximum performance at lower luminescence (less than 100 cd/m²). Moreover, pyrene-pyridine-based devices showed low roll-off as compared to the reference device. For example, with an increase in luminescence from 1000 to 10 000 cd/m², the devices with Py-Br and Py-MeO demonstrated 6 and 53% roll-off. Furthermore, the devices with Py-Me and Py-03 showed efficiency roll-up in device performance while moving from 1000 to 10 000 cd/m². However, the reference device (NPB) showed the highest efficiency roll-off (58%) while switching to higher luminescence.

Interestingly, these devices demonstrated efficiency roll-up behavior at higher voltage and brightness, unlike typical OLED devices, in which the roll-off phenomenon is inevitable. The

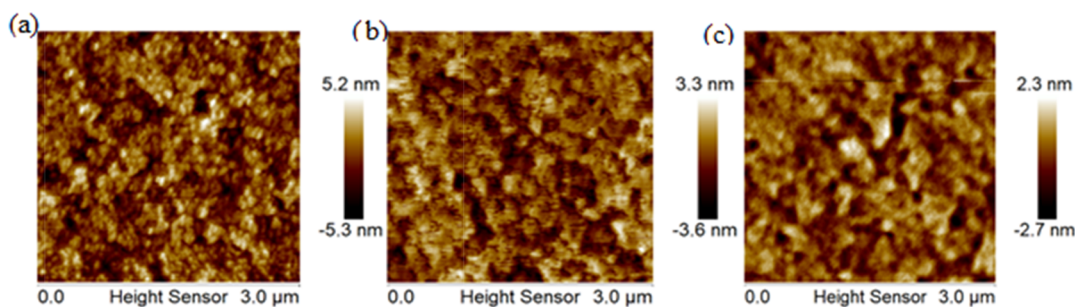


Figure 5. AFM topography images of (a) PEDOT:PSS, (b) HTL on PEDOT:PSS, and (c) EML on PEDOT:PSS and HTL.

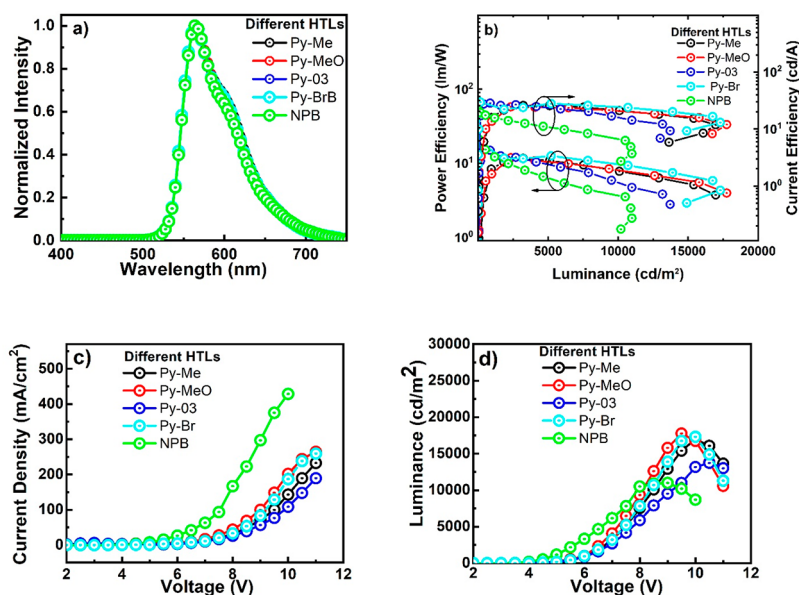


Figure 6. Electroluminescence properties of different HTL-enabled OLEDs. (a) Electroluminescence spectrum of OLED devices consisting of different HTLs. (b) Power efficiency–luminescence–current efficiency plot. (c) Current density–voltage plot. (d) Luminescence–voltage plot.

Table 2. Performance Summary of OLED Devices with Different HTLs

HTL	V_{on}^a (V)	PE ^b (lm/W)	CE ^c (cd/A)	EQE ^d (%)	CIE ^e	max luminance (cd/m ²)
@ 1000/10 000 cd/m ² /maximum						
Py-Me	3	8.5/7.8/11.4	16.3/21.1/25.2	5.6/6.8/8.5	(0.51, 0.49)/(0.51, 0.49)	16 970
Py-MeO	3	10.3/3/11.8	19.2/9/25.7	6.9/2.9/8.8	(0.51, 0.49)/(0.51, 0.49)	15 270
Py-03	3	8.4/6.3/11.8	16/17.3/26.6	5/5.2/8.5	(0.51, 0.49)/(0.51, 0.49)	13 720
Py-Br	3	11.7/7.9/12.3	22.4/21/27.6	7.4/6.6/9.0	(0.5, 0.49)/(0.5, 0.5)	17 300
NPB	3	10.5/2.7/20.3	16.2/6.7/20.7	5.1/2.1/6.7	(0.5, 0.5)/(0.5, 0.5)	10 980

^aTurn-on voltage. ^bPower efficiency. ^cCurrent efficiency. ^dExternal quantum efficiency. ^eCIE_{xy} coordinates at 1000 and 10 000 cd/m².

reason behind this may be attributed to (i) balanced charge carrier transport in the radiative recombination zone and (ii) the paired host and guest energy levels in the emissive layer, allowing excitons to generate mostly on the guest at low voltage, but with increasing exciton generation on the host as the voltage increases, enabling possibilities of utilizing all of the recombination sites generated in an emissive layer.⁶⁸ The designed device structure favors the formation of the majority of excitons on the dopant at low bias because the barrier for the hole to enter the host is comparatively higher. The generated low-energy excitons could not trigger the high energy emission of the dopant molecules, hence poor device performance. At high voltage, holes with higher energy could easily overcome the hole injection barrier between HTL and host and increase the possibility of an enhanced amount of exciton formation on the host molecules. Typically, the excitons generated on the host molecule possess exciting energy higher than that of those generated on the guest. Due to appropriate energy levels between the employed host–guest system, these generated excitons efficiently transferred to the guest, hence showing better device performance at a higher voltage or luminance.

To get a better understanding of balanced charge-transport properties in the emissive layer, the hole-only devices (HODs) have been fabricated with the following device structure ITO/PEDOT:PSS (35 nm)/HTM (25 nm)/LiF (1 nm)/Al (100 nm). The J – V characteristics of the HOD are displayed in

Figure 7. It is interesting to note that higher current density is observed for all of the pyrene–pyridine-based hole-trans-

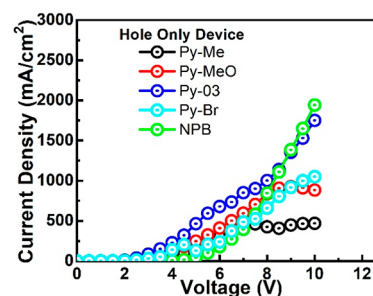


Figure 7. Current density vs voltage curves of the hole-only devices (HODs).

porting materials as compared to NPB-based reference devices till 7 V. Among all, the Py-03-based device demonstrated the highest current density at operating voltage, followed by the device with Py-MeO. High current density in hole-only devices might be attributed to better carrier transport by reducing the energy barrier. Furthermore, the pyrene–pyridine HTL-based OLED devices favor the injection of holes to the host matrix when compared with NPB-based reference devices because of the comparatively low hole injection barrier between reported new HTL molecules and employed host material CBP. Recently, Yadav et al. also reported that the energy barrier

lesser than/equal to 0.4 eV with respect to the emission layer facilitates a better hole transport from a hole injection layer to the emissive layer, which in turn improves the exciton generation in the emissive layer.⁶⁹ Since the pyridine and bromobenzene units have electron-withdrawing abilities, the electron-only devices (EODs) have also been fabricated with the following device architecture: ITO/PEDOT:PSS (35 nm)/TPBi (20 nm)/HTM (25 nm)/TPBi (35 nm)/LiF (1 nm)/Al (100 nm) to investigate the effect of substitutional units in Py-03, Py-MeO, Py-Me, and Py-Br on the electron transport properties of the synthesized molecules. The J - V characteristics of EOD show that Py-Br has better electron mobility as compared to other counterparts (Figure S30).

High performance of the OLED can be realized by the effective utilization of radiative exciton, which can be achieved using a suitable hole-transporting material with high triplet energy. This prevents the exciton energy transfer from the host to the hole-transporting layer and maintains the position of the recombination zone.⁷⁰ Also, pyrene-pyridine-based hole-transporting materials demonstrate a better electron blocking layer as compared to NPB. The relatively higher triplet energy of Py-Br (2.62 eV) than that of the host material (CBP) possibly helps in confining the triplet excitons within the emission layer most effectively as compared to NPB-based devices, resulting in improved device performance of Py-Br (Figure 8).

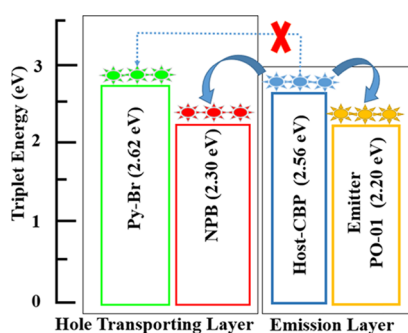


Figure 8. Schematic illustration of exciton energy transfer with the triplet energy level of different HTMs.

Further, the devices with Py-Me and Py-03 demonstrated an improvement in device performance at higher voltage and luminescence. To understand these characteristics at a molecular level, we analyzed the single-crystal structures of

Py-Me and Py-03 (Figure 1). The molecular-level understanding was important to establish a structure-emission relationship. The single crystals of Py-03 and Py-Me (Figures S5–S16) were grown in a DCM/MeOH (2:1) mixed solvent by the slow evaporation method and were studied in detail. The crystal refinement data are listed in Tables S1 and S2. Despite our efforts, we could not isolate single crystals of Py-Br and Py-MeO. The ORTEP diagrams of Py-03 and Py-Me are shown in Figure 1. The single-crystal analysis showed that Py-03 and Py-Me corresponded to the monoclinic and orthorhombic systems having space groups $P2_1$ and $Pca2_1$, respectively. The crystal structure analysis of these two compounds helped us to understand that there was no π - π stacking between the neighboring molecules. It was observed that the pyridine unit is tilted to the pyrene ring plane at an angle of 66.80° in Py-03 and 68.75° in Py-Me (Figures 9, S6, and S14). The tilted pyridine ring in the molecule barred the neighboring molecules from coming together in the solid state such that the π - π stacking was negligible. Instead, the distance between two neighboring pyrene rings in Py-03 is 5.723 \AA (Figure S5), which indicates that these rings are far from each other. Due to the large dihedral angle between pyrene and pyridine rings, pyrene lacks electronic π -conjugation with the pyridine unit, hence, the flow of the π -electron from pyrene to pyridine is severely restricted. The dihedral angles between the pyridine and two phenyl groups are different in both the molecules, indicating that these phenyl rings have a different degree of π -conjugation with the pyridine ring. In the case of Py-03, the angles between the two phenyl rings substituted with pyridine are 35.90 and 19.44° (Figures 9, S7, and S8), respectively, indicating that one phenyl ring is non-coplanar to the pyridine ring and the second one has some degree of coplanarity with the pyridine ring. Therefore, out of these two phenyl rings, one has some extent of π -conjugation with the pyridine ring, while the other one has very weak π -conjugation.

Similarly, in the case of Py-Me, the angles between two phenyl rings and pyridine are 24.12 and 11.55° (Figure 9), respectively. However, in the case of Py-Me, the angles between pyridine and these phenyl rings decrease by 11.78 and 7.89° compared to the angles between pyridine and phenyl rings of Py-03. Thus, both the phenyl rings are having better planarity and π -conjugation with the pyridine ring as compared to that of Py-03. Hence, due to the presence of different sorts of dihedral angles between the conjugating units, the π -conjugation in the whole molecule is not uniform, and therefore, the HOMO of the molecule is fully spread over the

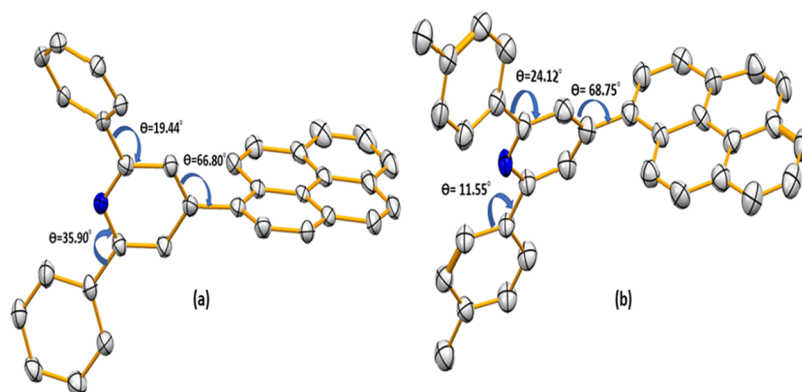


Figure 9. Angles between pyrene, pyridine, and phenyl rings in (a) Py-03 and (b) Py-Me.

pyrene ring (Figures 3 and S3). Also, the crystal structure analysis reveals the presence of various types of CH– π interactions with the neighboring molecules. The various distances of the short-range contacts in **Py-03** are 2.805 Å (between C2 and H2), 2.805 Å (between C3 and H2), 2.828 Å (between C3 and H23), 2.722 Å (between H23 and C4), as shown in Figure S9. Similarly, in **Py-Me**, the short-range contacts are 2.820 Å (between C69 and H01B), 2.350 Å (between H21 and H40), 2.854 Å (between C1 and H37), as shown in Figure S13. The crystal packing structures of **Py-03** and **Py-Me** are displayed in Figures S5 and S10–S12, respectively. It is observed that both the molecules show a similar type of crystal packing; pyrene was packed in the first layer on the head side and the pyridine was seated on the head side in the second layer.

The absence of π – π stacking in solid-state, donor–acceptor properties of molecules (**Py-Me** and **Py-03**), and the less π -electron flow from pyrene to pyridine might help in achieving the balanced carrier transport, which results in obtaining high stability and improved device performance at a higher voltage. While the large dihedral angle between pyrene and pyridine rings is restricting π -conjugation between them and avoiding π – π stacking of the neighboring molecules due to a bent structure, the presence of electron-withdrawing pyridine functionality helps in tuning overall molecular energy levels and possibly makes the hole extraction and transport process more effective.⁵⁴

Carrier injection and carrier-transporting ability of a material are important characteristics in determining OLED performance and stability. In specific, hole injection and transporting characteristics are important factors for determining barrier-free injection, reducing the charge accumulation, maintaining the charge balance for effective recombination, and reducing the efficiency roll-off. In this study, we demonstrate a new series of pyrene–pyridine-based hole-transporting material with suitable molecular orbital energy levels for barrier-free transport, balanced mobility for effective recombination, and high triplet energy for confining the excitons in the emission layer. These pyrene–pyridine-based hole-transporting materials enabled devices to demonstrate stable performance with low roll-off. Moreover, high thermal stability also plays a dominant role in achieving device stability. Further, the device with **Py-Me** and **Py-03** demonstrated efficiency roll-up in device performance while moving from 1000 to 10 000 cd/m². All of the devices with our new HTMs showed higher luminance as compared to NPB-based devices.

CONCLUSIONS

In summary, we have designed and synthesized a library of new functional pyrene–pyridine-integrated four molecular systems, viz., **Py-03**, **Py-MeO**, **Py-Me**, and **Py-Br** through adaptation of a simple condensation method with good yield. The absence of π – π stacking in the solid state and donor–acceptor properties were established by the single-crystal structure analyses of two compounds. It has been shown that both the optical and electrochemical properties of these materials entrust them as hole-transporting materials to be used in OLED applications. All of the synthesized molecules showed high triplet energy, high thermal stability, suitable molecular energy levels, good solubility in most of the organic solvents, and suitable ionization potential to make them a good hole transporter. All of the compounds were tested as hole-transporting layers in multilayer OLED devices, and it was found that the device with

a hole-transporting layer of **Py-Br** offered the highest performance (a maximum luminance of 17 300 cd/m², a maximum current efficiency 27.6 cd/A, and a maximum EQE 9% at 3500 cd/m² with 7% roll-off from 1000 to 10 000 cd/m²). We believe that the present pyrene–pyridine-based materials could be promising hole-transporting materials for future applications in OLEDs.

EXPERIMENTAL SECTION

Solution Preparation. The solution of HTL (**Py-03**, **Py-MeO**, **Py-Me**, **Py-Br**), host (CBP) (4,4'-bis(*N*-carbazolyl)-1,1'-biphenyl), and emitter (PO-01) (iridium(III) bis(4-phenylthieno[3,2-*c*]pyridinato-*N,C2'*)acetylacetonate) materials was prepared by dissolving them in tetrahydrofuran (THF) solvent at 40 °C for 0.5 h via an ultrasonication process. The concentrations of host and guest molecules are 10 and 1 mg/mL, respectively. The emissive layer is prepared by blending host and guest material solutions in an appropriate amount.

Substrate Cleaning. All of the solution-processed OLED devices were fabricated on a glass substrate with a patterned ITO, which is 125 nm thick. After cleaning with a detergent solution, the ITO glasses were cleaned for 30 min sequentially in acetone and isopropanol by an ultrasonic bath at temperatures of 50 °C and 60 °C, respectively, and treated with UV-O₃ for 20 min.

Device Fabrication. OLED devices were fabricated on a 125 nm ITO-patterned glass substrate. A 30 nm layer of 3,4-ethylenedioxythiophene-poly(styrenesulfonate) (PEDOT:PSS) was spin-coated at 4500 rpm for 20 s and then dried at 130 °C for 20 min. Further, the hole-transporting materials were completely dissolved in tetrahydrofuran (THF); a 25 nm layer of hole-transporting materials was spin-coated (2500 rpm for 20 s) and dried at 70 °C for 20 min. CBP (4,4'-bis(*N*-carbazolyl)-1,1'-biphenyl) as a host and 12.5 wt % of PO-01 (iridium(III) bis(4-phenylthieno[3,2-*c*]pyridinato-*N,C2'*)acetylacetonate) as an emitter material were dissolved in (THF) and a 20 nm of emissive layer was spin-coated at 2500 rpm for 20 s. The spin coating of all layers was performed in a nitrogen atmosphere inside a glovebox. A 30 nm layer of TPBi (2,2',2''-(1,3,5-benzinetriyl)-tris(1-phenyl-1-*H*-benzimidazole)) as an electron transporting layer, 1 nm of LiF (lithium fluoride) as an electron injection layer, and 150 nm of aluminum were deposited by thermal evaporation under high vacuum (5×10^{-6} Torr). A similar fabrication process was followed for making OLEDs with NPB (*N,N'*-di(1-naphthyl)-*N,N'*-diphenyl-(1,1'-biphenyl)-4,4'-diamine) as a reference hole-transporting material.

Synthetic Procedure and Characterization of **Py-03, **Py-MeO**, **Py-Me**, and **Py-Br**.** Procedure for the Synthesis of 2,6-Diphenyl-4-(pyren-1-yl)pyridine (**Py-03**). A mixture of acetophenone (3 equiv), 1-pyrenecarboxaldehyde (1 equiv), NaOH (3 equiv), and EtOH (15 mL) in 100 mL of RB was stirred at room temperature for 1 h. After that, the reaction mixture was refluxed at 80 °C for 1 h. Then, ammonium acetate (8 equiv) was added and the reaction mixture was refluxed for 12 h. In the end, the reaction mixture was quenched with water and extracted with DCM. The organic layer was then washed with water (2 × 25 mL) and dried over sodium sulfate. The organic solvent was evaporated using a rotaevaporator, and the crude solid was purified by column chromatography with 3% ethylacetate–hexane as the eluent; white solid; yield: 60%; ¹H NMR (500 MHz, CDCl₃): 7.42–7.44 (t, *J* = 7.5 Hz, 2H), 7.48–7.51 (t, *J* = 7.5 Hz, 4H), 7.94 (s,

2H), 7.97–8.02 (m, 3H), 8.06–8.10 (m, 2H), 8.14–8.24 (m, 8H); ^{13}C NMR (125 MHz, CDCl_3): 120.60, 124.41, 124.70, 124.75, 124.89, 125.23, 125.53, 126.21, 126.90, 127.14, 127.29, 127.99, 128.23, 128.73, 129.11, 130.79, 131.33, 135.12, 139.38, 150.67, 156.95; HRMS (ESI): calcd for $\text{C}_{33}\text{H}_{21}\text{N}$ [$\text{M} + \text{H}^+$]: 432.1746, found: 432.1746; mp: (observed from DSC) 190 °C.

Procedure for the Synthesis of 2,6-Bis(4-methoxyphenyl)-4-(pyren-1-yl)pyridine (Py-MeO). A mixture of 4-methoxyacetophenone (3 equiv), 1-pyrenecarboxaldehyde (1 equiv), NaOH (3 equiv), and EtOH (15 mL) in 100 mL of RB was stirred at room temperature for 1 h. After that, the reaction mixture was refluxed at 80 °C for 1 h. Then, ammonium acetate (8 equiv) was added and the reaction mixture was refluxed for 12 h. In the end, the reaction mixture was quenched with water and extracted with DCM. The organic layer was then washed with water (2×25 mL) and dried over sodium sulfate. The organic solvent was evaporated using a rotaevaporator, and the crude solid was purified by column chromatography with 4% ethylacetate–hexane as the eluent; white solid; yield: 65%; ^1H NMR (500 MHz, CDCl_3): 3.8 (s, 6H), 6.96–6.98 (d, $J = 8.2$, 4H), 7.76 (s, 2H), 7.92–8.15 (m, 13H); ^{13}C NMR (125 MHz, CDCl_3): 55.27, 113.98, 119.10, 124.51, 124.84, 125.13, 125.42, 126.15, 126.84, 127.27, 127.85, 128.07, 128.22, 128.34, 130.78, 131.17, 131.31, 132.08, 135.43, 150.37, 156.36, 160.46; HRMS (ESI): calcd for $\text{C}_{35}\text{H}_{25}\text{NO}_2$ [$\text{M} + \text{H}^+$]: 492.1958, found: 492.1958; mp: (observed from DSC) 200 °C.

Procedure for the Synthesis of 4-(Pyren-1-yl)-2,6-di-p-tolylpyridine (Py-Me). A mixture of 4-methylacetophenone (3 equiv), 1-pyrenecarboxaldehyde (1 equiv), NaOH (3 equiv), and EtOH (15 mL) in 100 mL of RB was stirred at room temperature for 1 h. After that, the reaction mixture was refluxed at 80 °C for 1 h. Then, ammonium acetate (8 equiv) was added and the reaction mixture was refluxed for 12 h. In the end, the reaction mixture was quenched with water and extracted with DCM. The organic layer was then washed with water (2×25 mL) and dried over sodium sulfate. The organic solvent was evaporated using a rotaevaporator, and the crude solid was purified by column chromatography with 2% ethylacetate–hexane as the eluent; white solid; yield: 55%; ^1H NMR (500 MHz, CDCl_3): 2.30 (t, 6H), 7.19–7.17 (d, $J = 8.25$, 4H), 7.77 (s, 2H), 7.90–7.86 (m, 3H), 7.96–7.96 (d, $J = 2.75$, 2H) 8.03–8.01 (d, $J = 3.25$, 5H), 8.10–8.06 (m, 3H); ^{13}C NMR (125 MHz, CDCl_3): 21.30, 119.99, 124.51, 124.72, 124.88, 125.17, 125.45, 126.17, 126.90, 126.99, 127.29, 127.90, 128.13, 128.25, 129.42, 130.81, 131.24, 131.33, 135.35, 136.69, 139.02, 150.45, 156.86; HRMS (ESI): calcd for $\text{C}_{35}\text{H}_{25}\text{N}$ [$\text{M} + \text{H}^+$]: 460.2059, found: 460.2059; mp: (observed from DSC) 210 °C.

Procedure for the Synthesis of 2,6-Bis(4-bromophenyl)-4-(pyren-1-yl)pyridine (Py-Br). A mixture of 4-bromoacetophenone (3 equiv), 1-pyrenecarboxaldehyde (1 equiv), NaOH (3 equiv), and EtOH (15 mL) in 100 mL of RB was stirred at room temperature for 1 h. After that, the reaction mixture was refluxed at 80 °C for 1 h. Then, ammonium acetate (8 equiv) was added, and the reaction was refluxed for 12 h. In the end, the reaction mixture was quenched with water and extracted with DCM. The organic layer was then washed with water (2×25 mL) and dried over sodium sulfate. The organic solvent was evaporated using a rotaevaporator, and the crude solid was purified by column chromatography with 2% ethylacetate–hexane as the eluent; light green solid; yield: 55%; ^1H NMR

(500 MHz, CDCl_3): 7.64–7.63 (brs, 4H), 7.93–8.25 (m, 15H); ^{13}C NMR (125 MHz, CDCl_3): 120.41, 124.22, 124.55, 124.70, 125.03, 125.33, 126.02, 126.71, 126.94, 127.09, 127.79, 128.03, 128.53, 128.91, 130.60, 131.12, 134.93, 139.18, 150.48, 156.76; HRMS (ESI): calcd for $\text{C}_{33}\text{H}_{19}\text{Br}_2\text{N}$ [M^+]: 589.9939, found: 589.9939; mp: (observed from DSC) 245 °C.

■ ASSOCIATED CONTENT

Supporting Information

The Supporting Information is available free of charge at <https://pubs.acs.org/doi/10.1021/acsomega.0c04080>.

Detail information of instruments used during the analysis, cyclic voltammetry, TGA/DSC analysis, DFT (HOMO/LUMO) distribution, TD spectra, X-ray diffraction studies, ^1H and ^{13}C NMR spectra, mass spectra, and triplet energy levels measurements and calculations (PDF)

■ AUTHOR INFORMATION

Corresponding Authors

Jwo-Huei Jou – Department of Materials Science and Engineering, National Tsing Hua University, Hsinchu 30013, Taiwan, R.O.C.; orcid.org/0000-0002-9413-0206; Email: jjou@mx.nthu.edu.tw

Subrata Ghosh – School of Basic Sciences, IIT Mandi, Mandi, Himachal Pradesh 175005, India; orcid.org/0000-0002-8030-4519; Email: subrata@iitmandi.ac.in

Authors

Krishan Kumar – School of Basic Sciences, IIT Mandi, Mandi, Himachal Pradesh 175005, India

Kiran Kishore Kesavan – Department of Materials Science and Engineering, National Tsing Hua University, Hsinchu 30013, Taiwan, R.O.C.

Diksha Thakur – School of Basic Sciences, IIT Mandi, Mandi, Himachal Pradesh 175005, India

Subrata Banik – Department of Chemistry, School of Chemical and Biotechnology, SASTRA Deemed University, Thanjavur 613401, Tamil Nadu, India; orcid.org/0000-0001-5155-3957

Jayachandran Jayakumar – Department of Chemistry, National Tsing Hua University, Hsinchu 30013, Taiwan, R.O.C.; orcid.org/0000-0003-3135-1535

Chien-Hong Cheng – Department of Chemistry, National Tsing Hua University, Hsinchu 30013, Taiwan, R.O.C.; orcid.org/0000-0003-3838-6845

Complete contact information is available at: <https://pubs.acs.org/doi/10.1021/acsomega.0c04080>

Author Contributions

† K.K. and K.K.K. contributed equally to this work.

Notes

The authors declare no competing financial interest.

■ ACKNOWLEDGMENTS

Financial support from Uchytar Avishkar Yojana (UAY) is thankfully acknowledged. S.G., D.T., and K.K. acknowledge the research facility of the Advanced Materials Research Center (AMRC), IIT Mandi. Dr. Deepak Kumar Dubey is thankfully acknowledged for his kind help during manuscript revision.

REFERENCES

- (1) Tang, C. W.; Vanslyke, S. A. Organic Electroluminescent Diodes. *Appl. Phys. Lett.* **1987**, *51*, 913–915.
- (2) Chidirala, S.; Ulla, H.; Valaboju, A.; Kiran, M. R.; Mohanty, M. E.; Satyanarayan, M. N.; Umesh, G.; Bhanuprakash, K.; Rao, V. J. Pyrene-Oxadiazoles for Organic Light-Emitting Diodes: Triplet to Singlet Energy Transfer and Role of Hole-Injection/Hole-Blocking Materials. *J. Org. Chem.* **2016**, *81*, 603–614.
- (3) Jung, H.; Kang, S.; Lee, H.; Yu, Y. J.; Jeong, J. H.; Song, J.; Jeon, Y.; Park, J. High Efficiency and Long Lifetime of a Fluorescent Blue-Light Emitter Made of a Pyrene Core and Optimized Side Groups. *ACS Appl. Mater. Interfaces* **2018**, *10*, 30022–30028.
- (4) Lee, D. R.; Choi, J. M.; Lee, C. W.; Lee, J. Y. Ideal Molecular Design of Blue Thermally Activated Delayed Fluorescent Emitter for High Efficiency, Small Singlet-Triplet Energy Splitting, Low Efficiency Roll-off, and Long Lifetime. *ACS Appl. Mater. Interfaces* **2016**, *8*, 23190–23196.
- (5) Schwartz, G.; Pfeiffer, M.; Reineke, S.; Walzer, K.; Leo, K. Harvesting Triplet Excitons from Fluorescent Blue Emitters in White Organic Light-Emitting Diodes. *Adv. Mater.* **2007**, *19*, 3672–3676.
- (6) Kim, H. G.; Kim, K. H.; Kim, J. J. Highly Efficient, Conventional, Fluorescent Organic Light-Emitting Diodes with Extended Lifetime. *Adv. Mater.* **2017**, *29*, No. 1702159.
- (7) Reineke, S.; Thomschke, M.; Lüssem, B.; Leo, K. White Organic Light-Emitting Diodes: Status and Perspective. *Rev. Mod. Phys.* **2013**, *85*, 1245–1293.
- (8) Kumar Konidena, R.; Justin Thomas, K. R.; Kumar Dubey, D.; Sahoo, S.; Jou, J. H. A New Molecular Design Based on Hybridized Local and Charge Transfer Fluorescence for Highly Efficient (>6%) Deep-Blue Organic Light Emitting Diodes. *Chem. Commun.* **2017**, *53*, 11802–11805.
- (9) Forrest, S. R.; Thompson, M. E. Introduction: Organic Electronics and Optoelectronics. *Chem. Rev.* **2007**, *107*, 923–925.
- (10) Jou, J. H.; Li, J. L.; Sahoo, S.; Dubey, D. K.; Kumar Yadav, R. A.; Joseph, V.; Thomas, K. R. J.; Wang, C. W.; Jayakumar, J.; Cheng, C. H. Enabling a 6.5% External Quantum Efficiency Deep-Blue Organic Light-Emitting Diode with a Solution-Processable Carbazole-Based Emitter. *J. Phys. Chem. C* **2018**, *122*, 24295–24303.
- (11) Jou, J. H.; Kumar, S.; Agrawal, A.; Li, T. H.; Sahoo, S. Approaches for Fabricating High Efficiency Organic Light Emitting Diodes. *J. Mater. Chem. C* **2015**, *3*, 2974–3002.
- (12) Baldo, M. A.; O'Brien, D. F.; You, Y.; Shoustikov, A.; Sibley, S.; Thompson, M. E.; Forrest, S. R. Highly Efficient Phosphorescent Emission from Organic Electroluminescent Devices. *Nature* **1998**, *395*, 151–154.
- (13) Kido, J.; Kimura, M.; Nagai, K. Multilayer White Light-Emitting Organic Electroluminescent Device. *Science* **1995**, *267*, 1332–1334.
- (14) Konidena, R. K.; Thomas, K. R. J.; Pathak, A.; Dubey, D. K.; Sahoo, S.; Jou, J. H. Tuning the Photophysical and Electroluminescence Properties in Asymmetrically Tetrasubstituted Bipolar Carbazoles by Functional Group Disposition. *ACS Appl. Mater. Interfaces* **2018**, *10*, 24013–24027.
- (15) Burroughes, J. H.; Bradley, D. D. C.; Brown, A. R.; Marks, R. N.; Mackay, K.; Friend, R. H.; Burns, P. L.; Holmes, A. B. Light-Emitting Diodes Based on Conjugated Polymers. *Nature* **1990**, *347*, 539–541.
- (16) Huang, J.; Su, J. H.; Tian, H. The Development of Anthracene Derivatives for Organic Light-Emitting Diodes. *J. Mater. Chem.* **2012**, *22*, 10977–10989.
- (17) Tokito, S.; Tanaka, H.; Noda, K.; Okada, A.; Taga, Y. Thermal Stability in Oligomeric Triphenylamine/Tris(8-Quinololato) Aluminum Electroluminescent Devices. *Appl. Phys. Lett.* **1997**, *70*, 1929–1931.
- (18) (a) Joswick, M. D.; Campbell, I. H.; Barashkov, N. N.; Ferraris, J. P. Systematic Investigation of the Effects of Organic Film Structure on Light Emitting Diode Performance. *J. Appl. Phys.* **1996**, *80*, 2883–2890. (b) Han, E. M.; Do, L. M.; Yamamoto, N.; Fujihira, M. Crystallization of Organic Thin Films for Electroluminescent Devices. *Thin Solid Films* **1996**, *273*, 202–208. (c) Shen, J. Y.; Lee, C. Y.; Huang, T. H.; Lin, J. T.; Tao, Y. T.; Chien, C. H.; Tsai, C. High Tg Blue Emitting Materials for Electroluminescent Devices. *J. Mater. Chem.* **2005**, *15*, 2455–2463.
- (19) Huang, J.; Su, J. H.; Li, X.; Lam, M. K.; Fung, K. M.; Fan, H. H.; Cheah, K. W.; Chen, C. H.; Tian, H. Bipolar Anthracene Derivatives Containing Hole- and Electron-Transporting Moieties for Highly Efficient Blue Electroluminescence Devices. *J. Mater. Chem.* **2011**, *21*, 2957–2964.
- (20) (a) Wong, W. Y.; Ho, C. L. Functional Metallophosphors for Effective Charge Carrier Injection/Transport: New Robust OLED Materials with Emerging Applications. *J. Mater. Chem.* **2009**, *19*, 4457–4482. (b) Yu, M. X.; Duan, J. P.; Lin, C. H.; Cheng, C. H.; Tao, Y. T. Diaminoanthracene Derivatives as High-Performance Green Host Electroluminescent Materials. *Chem. Mater.* **2002**, *14*, 3958–3963.
- (21) Zheng, Z.; Dong, Q.; Gou, L.; Su, J. H.; Huang, J. Novel Hole Transport Materials Based on N,N'-Disubstituted-Dihydrophenazine Derivatives for Electroluminescent Diodes. *J. Mater. Chem. C* **2014**, *2*, 9858–9865.
- (22) Jhulki, S.; Moorthy, J. N. Small Molecular Hole-Transporting Materials (HTMs) in Organic Light-Emitting Diodes (OLEDs): Structural Diversity and Classification. *J. Mater. Chem. C* **2018**, *6*, 8280–8325.
- (23) Kulkarni, A. P.; Tonzola, C. J.; Babel, A.; Jenekhe, S. A. Electron Transport Materials for Organic Light-Emitting Diodes. *Chem. Mater.* **2004**, *16*, 4556–4573.
- (24) Liu, Q. De.; Lu, J.; Ding, J.; Day, M.; Tao, Y.; Barrios, P.; Stupak, J.; Chan, K.; Li, J.; Chi, Y. Monodisperse Starburst Oligofluorene-Functionalized 4,4',4''-Tris(Carbazol-9-Yl)-Triphenylamines: Their Synthesis and Deep-Blue Fluorescence Properties for Organic Light-Emitting Diode Applications. *Adv. Funct. Mater.* **2007**, *17*, 1028–1036.
- (25) Kuwabara, Y.; Ogawa, H.; Inada, H.; Noma, N.; Shiota, Y. Thermally Stable Multilayered Organic Electroluminescent Devices Using Novel Starburst Molecules, 4,4',4''-Tri(N-carbazolyl)-Triphenylamine (TCTA) and 4,4',4''-Tris(3-methylphenylphenylamino)Triphenylamine (m-MTDATA), as Hole-transport Materials. *Adv. Mater.* **1994**, *6*, 677–679.
- (26) Hamlen, S. Advanced Materials. *Offshore Eng.* **2017**, *42*, 38–39.
- (27) Grigalevicius, S.; Tavgeniene, D.; Krucaite, G.; Griniene, R.; Li, W. C.; Luo, D.; Chang, C. H. 9,9'-Bis(2,2-Diphenylvinyl)[3,3']-Bicarbazole as Low Cost Efficient Hole Transporting Material for Application in Red PhOLEDs. *Dyes Pigm.* **2018**, *152*, 100–104.
- (28) Krucaite, G.; Volyniuk, D.; Simokaitiene, J.; Grigalevicius, S.; Lin, C. H.; Shao, C. M.; Chang, C. H. Naphthyl Substituted Triphenylamine Derivatives as Hole Transporting Materials for Efficient Red PhOLEDs. *Dyes Pigm.* **2019**, *162*, 196–202.
- (29) Wu, F. I.; Shih, P. I.; Yuan, M. C.; Dixit, A. K.; Shu, C. F.; Chung, Z. M.; Diao, E. W. G. Novel Distyrylcarbazole Derivatives as Hole-Transporting Blue Emitters for Electroluminescent Devices. *J. Mater. Chem.* **2005**, *15*, 4753–4760.
- (30) Kotchpradist, P.; Prachumrak, N.; Tarsang, R.; Jungsuttiwong, S.; Keawin, T.; Sudyoadsuk, T.; Promarak, V. Pyrene-Functionalized Carbazole Derivatives as Non-Doped Blue Emitters for Highly Efficient Blue Organic Light-Emitting Diodes. *J. Mater. Chem. C* **2013**, *1*, 4916–4924.
- (31) O'Brien, D. F.; Burrows, P. E.; Forrest, S. R.; Koene, B. E.; Loy, D. E.; Thompson, M. E. Hole Transporting Materials with High Glass Transition Temperatures for Use in Organic Light-Emitting Devices. *Adv. Mater.* **1998**, *10*, 1108–1112.
- (32) Sipaviciute, D.; Tavgeniene, D.; Krucaite, G.; Volyniuk, D.; Grazulevicius, J. V.; Yao, B.; Xie, Z.; Zhang, B.; Grigalevicius, S. 3,7-Diaryl Substituted 10-Butylphenoxazines as New Hole Transporting Materials for Organic Light Emitting Devices. *Dyes Pigm.* **2017**, *137*, 208–213.
- (33) Lee, J.; Chopra, N.; Eom, S. H.; Zheng, Y.; Xue, J.; So, F.; Shi, J. Effects of Triplet Energies and Transporting Properties of Carrier

Transporting Materials on Blue Phosphorescent Organic Light Emitting Devices. *Appl. Phys. Lett.* **2008**, *93*, No. 123306.

(34) Huang, Q.; Evmenenko, G. A.; Dutta, P.; Lee, P.; Armstrong, N. R.; Marks, T. J. Covalently Bound Hole-Injecting Nanostructures. Systematics of Molecular Architecture, Thickness, Saturation, and Electron-Blocking Characteristics on Organic Light-Emitting Diode Luminance, Turn-on Voltage, and Quantum Efficiency. *J. Am. Chem. Soc.* **2005**, *127*, 10227–10242.

(35) Borsenberger, P. M.; Magin, E. H.; Fitzgerald, J. J. Hole Transport in 1,1-Bis((Di-4-Tolylamino)Phenyl)Cyclohexane (TAPC) Doped Poly(Styrene)S. *J. Phys. Chem. A* **1993**, *97*, 8250–8253.

(36) Zhang, Q.; Chen, J.; Cheng, Y.; Wang, L.; Ma, D.; Jing, X.; Wang, F. Novel Hole-Transporting Materials Based on 1,4-Bis-(Carbazolyl)Benzene for Organic Light-Emitting Devices. *J. Mater. Chem.* **2004**, *14*, 895–900.

(37) Okumoto, K.; Shirota, Y. Development of High-Performance Blue-Violet-Emitting Organic Electroluminescent Devices. *Appl. Phys. Lett.* **2001**, *79*, 1231–1233.

(38) (a) Dubey, D. K.; Swayamprabha, S. S.; Kumar Yadav, R. A.; Tavgeniene, D.; Volyniuk, D.; Grigalevicius, S.; Jou, J. H. A Thermally Cross-Linkable Hole-Transporting Small-Molecule for Efficient Solution-Processed Organic Light Emitting Diodes. *Org. Electron.* **2019**, *73*, 94–101. (b) Dubey, D. K.; Yadav, R. A. K.; Tavgeniene, D.; Grigalevicius, S.; Jou, J. H. Crosslinkable Hole-Transporting Small Molecule as a Mixed Host for Efficient Solution-Processed Red Organic Light Emitting Diodes. *Thin Solid Films* **2018**, *660*, 956–960.

(39) Wong, M. Y.; Zysman-Colman, E. Purely Organic Thermally Activated Delayed Fluorescence Materials for Organic Light-Emitting Diodes. *Adv. Mater.* **2017**, *29*, No. 1605444.

(40) Müllen, K.; Scherf, U. *Organic Light Emitting Devices: Synthesis, Properties and Applications*; John Wiley & Sons, 2006.

(41) Figueira-Duarte, T. M.; Müllen, K. Pyrene-Based Materials for Organic Electronics. *Chem. Rev.* **2011**, *111*, 7260–7314.

(42) Cui, B. B.; Zhu, C.; Yang, S.; Han, Y.; Yang, N.; Zhang, L.; Wang, Y.; Jia, Y.; Zhao, L.; Chen, Q. Two Low-Cost and Efficient Hole-Transporting Materials for n-i-p Type Organic-Inorganic Hybrid Perovskite Solar Cells. *ACS Omega* **2018**, *3*, 10791–10797.

(43) Chang, C. H.; Krucaite, G.; Lo, D.; Chen, Y. L.; Su, C. C.; Lin, T. C.; Grazulevicius, J. V.; Peculyte, L.; Grigalevicius, S. Naphthyl or Pyrenyl Substituted 2-Phenylcarbazoles as Hole Transporting Materials for Organic Light-Emitting Diodes. *Dyes Pigm.* **2017**, *136*, 302–311.

(44) Jeong, S. H.; Lee, K. H.; Lee, J. Y. Dual Role of a Pyrene Derivative as a Hole Transport Material and an Emitter in Blue Fluorescent Organic Light-Emitting Diodes. *Dyes Pigm.* **2019**, *171*, No. 107759.

(45) Salunke, J.; Singh, A.; He, D.; Pham, H. D.; Bai, Y.; Wang, L.; Dahlström, S.; Nyman, M.; Manzhos, S.; Feron, K.; Österbacka, R.; Priimagi, A.; Vivo, P.; Sonar, P. Fluorination of Pyrene-Based Organic Semiconductors Enhances the Performance of Light Emitting Diodes and Halide Perovskite Solar Cells. *Org. Electron.* **2020**, *77*, 105524.

(46) Keawin, T.; Prachumrak, N.; Namuangruk, S.; Pansay, S.; Kungwan, N.; Maensiri, S.; Jungsuttiwong, S.; Sudyoadsuk, T.; Promarak, V. Efficient Bifunctional Materials Based on Pyrene- and Triphenylamine-Functionalized Dendrimers for Electroluminescent Devices. *RSC Adv.* **2015**, *5*, 73481–73489.

(47) Thangthong, A. M.; Prachumrak, N.; Tarsang, R.; Keawin, T.; Jungsuttiwong, S.; Sudyoadsuk, T.; Promarak, V. Blue Light-Emitting and Hole-Transporting Materials Based on 9,9-Bis(4-Diphenylaminophenyl)Fluorenes for Efficient Electroluminescent Devices. *J. Mater. Chem.* **2012**, *22*, 6869–6877.

(48) Loy, D. E.; Koene, B. E.; Thompson, M. E. Thermally Stable Hole-Transporting Materials Based upon a Fluorene Core. *Adv. Funct. Mater.* **2002**, *12*, 245–249.

(49) Huang, P.; Manju, Kazim, S.; Sivakumar, G.; Salado, M.; Misra, R.; Ahmad, S. Pyridine Bridging Diphenylamine-Carbazole with Linking Topology as Rational Hole Transporter for Perovskite Solar Cells Fabrication. *ACS Appl. Mater. Interfaces* **2020**, *12*, 22881–22890.

(50) Liu, X.; Ma, S.; Ding, Y.; Gao, J.; Liu, X.; Yao, J.; Dai, S. Molecular Engineering of Simple Carbazole-Triphenylamine Hole Transporting Materials by Replacing Benzene with Pyridine Unit for Perovskite Solar Cells. *Sol. RRL* **2019**, *3*, No. 1800337.

(51) Xu, B.; Zhu, Z.; Zhang, J.; Liu, H.; Chueh, C. C.; Li, X.; Jen, A. K. Y. 4-Tert-Butylpyridine Free Organic Hole Transporting Materials for Stable and Efficient Planar Perovskite Solar Cells. *Adv. Energy Mater.* **2017**, *7*, No. 1700683.

(52) Reddy, S. S.; Arivunithi, V. M.; Sree, V. G.; Kwon, H.; Park, J.; Kang, Y. C.; Zhu, H.; Noh, Y. Y.; Jin, S. H. Lewis Acid-Base Adduct-Type Organic Hole Transport Material for High Performance and Air-Stable Perovskite Solar Cells. *Nano Energy* **2019**, *58*, 284–292.

(53) Duan, L.; Chen, Y.; Jia, J.; Zong, X.; Sun, Z.; Wu, Q.; Xue, S. Dopant-Free Hole-Transport Materials Based on 2,4,6-Triarylpyridine for Inverted Planar Perovskite Solar Cells. *ACS Appl. Energy Mater.* **2020**, *3*, 1672–1683.

(54) Wu, F.; Shan, Y.; Qiao, J.; Zhong, C.; Wang, R.; Song, Q.; Zhu, L. Replacement of Biphenyl by Bipyridine Enabling Powerful Hole Transport Materials for Efficient Perovskite Solar Cells. *ChemSusChem* **2017**, *10*, 3833–3838.

(55) Wazzan, N.; Safi, Z. Effect of Number and Position of Methoxy Substituents on Fine-Tuning the Electronic Structures and Photo-physical Properties of Designed Carbazole-Based Hole-Transporting Materials for Perovskite Solar Cells: DFT Calculations. *Arabian J. Chem.* **2019**, *12*, 1–20.

(56) Sallenave, X.; Shasti, M.; Anaraki, E. H.; Volyniuk, D.; Grazulevicius, J. V.; Zakeeruddin, S. M.; Mortezaali, A.; Grätzel, M.; Hagfeldt, A.; Sini, G. Interfacial and Bulk Properties of Hole Transporting Materials in Perovskite Solar Cells: Spiro-MeTAD versus spiro-OMeTAD. *J. Mater. Chem. A* **2020**, *8*, 8527–8539.

(57) Mimaite, V.; Grazulevicius, J. V.; Laurinaviciute, R.; Volyniuk, D.; Jankauskas, V.; Sini, G. Can Hydrogen Bonds Improve the Hole-Mobility in Amorphous Organic Semiconductors? Experimental and Theoretical Insights. *J. Mater. Chem. C* **2015**, *3*, 11660–11674.

(58) Schmidt, R.; Oh, J. H.; Sun, Y. S.; Deppisch, M.; Krause, A. M.; Radacki, K.; Braunschweig, H.; Könnemann, M.; Erk, P.; Bao, Z.; Würthner, F. High-Performance Air-Stable n-Channel Organic Thin Film Transistors Based on Halogenated Perylene Bisimide Semiconductors. *J. Am. Chem. Soc.* **2009**, *131*, 6215–6228.

(59) Tang, M. L.; Bao, Z. Halogenated Materials as Organic Semiconductors. *Chem. Mater.* **2011**, *23*, 446–455.

(60) Du, X.; Zhao, J.; Liu, W.; Wang, K.; Yuan, S.; Zheng, C.; Lin, H.; Tao, S.; Zhang, X. H. Bromine-Substituted Triphenylamine Derivatives with Improved Hole-Mobility for Highly Efficient Green Phosphorescent OLEDs with a Low Operating Voltage. *J. Mater. Chem. C* **2016**, *4*, 10301–10308.

(61) Krucaite, G.; Blazelevicius, D.; Tavgeniene, D.; Grigalevicius, S.; Lin, C. H.; Shao, C. M.; Chang, C. H. Tetramer of Triphenylamine and Similar Derivatives with Bromine Atoms as Hole Injecting/Transporting Materials for Efficient Red Phosphorescent OLEDs. *Opt. Mater.* **2020**, *108*, No. 110225.

(62) Yang, J. X.; Tao, X. T.; Chun, X. Y.; Yun, X. Y.; Wang, L.; Liu, Z.; Ren, Y.; Min, H. J. A Facile Synthesis and Properties of Multicarbazole Molecules Containing Multiple Vinylene Bridges. *J. Am. Chem. Soc.* **2005**, *127*, 3278–3279.

(63) Thakur, D.; Dubey, D. K.; Yadav, R. A. K.; Venkateswarulu, M.; Banik, S.; Jou, J. H.; Ghosh, S. Solution-Processed Hybrid Hosts: A Way to Explore High Triplet Energy with Admirable Current and Power Efficiency without Outcoupling Techniques for Phosphorescent OLEDs. *J. Mater. Chem. C* **2020**, *8*, 228–239.

(64) De Silva, T. P. D.; Youm, S. G.; Tamas, G. G.; Yang, B.; Wang, C. H.; Fronczek, F. R.; Sahasrabudhe, G.; Sterling, S.; Quarels, R. D.; Chhotaray, P. K.; Nesterov, E. E.; Warner, I. M. Pyrenylpyridines: Sky-Blue Emitters for Organic Light-Emitting Diodes. *ACS Omega* **2019**, *4*, 16867–16877.

(65) Wu, F.; Wang, L.; Tang, H.; Cao, D. Excited State Intramolecular Proton Transfer Plus Aggregation-Induced Emission-Based Diketopyrrolopyrrole Luminogen: Photophysical Properties

and Simultaneously Discriminative Detection of Trace Water in Three Organic Solvents. *Anal. Chem.* **2019**, *91*, 5261–5269.

(66) Zhao, Z.; Xu, X.; Wang, H.; Lu, P.; Yu, G.; Liu, Y. Zigzag Molecules from Pyrene-Modified Carbazole Oligomers: Synthesis, Characterization, and Application in OLEDs. *J. Org. Chem.* **2008**, *73*, 594–602.

(67) Giannetti, E. Thermal Stability and Bond Dissociation Energy of Fluorinated Polymers: A Critical Evaluation. *J. Fluorine Chem.* **2005**, *126*, 623–630.

(68) Jou, J. H.; Wang, Y. S.; Lin, C. H.; Shen, S. M.; Chen, P. C.; Tang, M. C.; Wei, Y.; Tsai, F. Y.; Chen, C. T. Nearly Non-Roll-off High Efficiency Fluorescent Yellow Organic Light-Emitting Diodes. *J. Mater. Chem.* **2011**, *21*, 12613–12618.

(69) Yadav, R. A. K.; Dubey, D. K.; Chen, S. Z.; Liang, T. W.; Jou, J. H. Role of Molecular Orbital Energy Levels in OLED Performance. *Sci. Rep.* **2020**, *10*, No. 9915.

(70) Dubey, D. K.; Krucaite, G.; Swayamprabha, S. S.; Yadav, R. A. K.; Blazelevicius, D.; Tagare, J.; Chavhan, S.; Hsueh, T. C.; Vaidyanathan, S.; Grigalevicius, S.; Jou, J. H. Fluorene Based Amorphous Hole Transporting Materials for Solution Processed Organic Light-Emitting Diodes. *Org. Electron.* **2020**, *79*, No. 105633.